Sensors **2002**, *2*, 91-110

sensors

ISSN 1424-8220

http://www.mdpi.net/sensors

Invited Paper

Room Temperature Ammonia and Humidity Sensing Using Highly Ordered Nanoporous Alumina Films

Elizabeth C. Dickey[1,*], Oomman K. Varghese[1], Keat G. Ong[2], Dawei Gong[2], Maggie Paulose[2] and Craig A. Grimes[2]

[1] Department of Materials Science & Engineering, The Pennsylvania State University, University Park, PA 16802

[2] Department of Electrical Engineering & Materials Research Institute, The Pennsylvania State University, University Park, PA 16802

* Author to whom correspondence should be addressed. Email: ecd10@psu.edu

Received: 9 February 2002 / Accepted: 1 March 2002 / Published: 18 March 2002

Abstract: The effect of pore size and uniformity on the response of nanoporous alumina, formed on aluminum thick films through an anodization process, to ammonia and humidity at room temperature is reported. Pore sizes examined range from 13 nm to 48 nm, with pore size standard deviations ranging from 2.6 nm to 7.8 nm. The response of the material to ammonia and humidity is a strong function of pore size and operating frequency. At 5 kHz an alumina sensor with an average pore size of 13.6 nm, standard deviation 2.6 nm, exhibits a factor of two change in impedance magnitude as it is cycled between an ammonia and argon environment. At 5 kHz the same sensor exhibits a well-behaved change in impedance magnitude of 10^3 over 20% to 90% relative humidity. Cole-Cole plots of the 5 Hz to 13 MHz measured impedance spectra, modeled using equivalent circuits, are used to resolve the effects of adsorption and ion migration.

Key words: Ammonia, Nanoporous, Impedance spectroscopy, Alumina, Humidity, Mesoporous.

Introduction

Both humidity and ammonia sensors have attracted considerable attention over many years due to their great importance in applications ranging from monitoring food quality to meteorological studies

[1-4]. Most humidity detection studies have focused on the use of polymer [1, 5-8] and ceramic materials [3, 9-20] due to their low cost and excellent performance. Ceramic humidity sensors are commercially available, and offer major advantages with high resistance to chemical attack, thermal stability, mechanical strength, and quick response. However ceramic humidity sensors still suffer from insufficient sensitivity over wide humidity ranges, as well as lack of reversibility and drift in base resistance with time due to the chemisorption of water molecules. Our interest is in developing reliable, high performance ceramic materials of large surface area for humidity and gas sensing. Therefore we have revisited the use of nanoporous alumina, a topic of considerable interest since the discovery of its moisture sensitive properties almost fifty years ago [21-32].

Ammonia sensors based upon polyaniline [33, 34], nafion [35], and polypyrrole-poly(vinyl alcohol) [36] thin film coatings have been reported. It is generally recognized that while polymers can offer a high degree of sensitivity, measurement drift and aging pose serious problems to polymer-based sensors. Earlier investigations on the use of thin-film ceramics for ammonia measurement include a SnO_2 sensor operating at 350°C [37], Pt and SiO_2 doped SnO_2 sensors operating at 160°C [38], a Pt doped $CdSnO_3$ sensor operating at 240°C [39], and TiO_2 based sensors operating at 300°C [40]. Our interest lies in room temperature sensing of ammonia using ceramic based sensors. As far as the authors are aware, this is the first reported observation of the ability to sense ammonia at room temperature (≈ 23°C) using a ceramic sensor, and the first reported use of Al_2O_3 for ammonia sensing. The fact we are able to measure ammonia concentrations using Al_2O_3 at room temperature makes possible a variety of new sensing applications, such as those associated with food safety.

Ceramic sensor operation is based on either electronic or ionic conductivity. The ability of alumina to sense humidity is based upon ionic conduction; the presence of an adsorbed layer of water at the surface reduces the total sensor impedance due to the increase in the ionic conductivity, as well as capacitance due to the high dielectric constant of water. Porous alumina is usually preferred for sensing applications due to the large surface area available for water adsorption. An additional advantage of porosity is that at a particular temperature and relative humidity (RH), water condensation occurs in pores up to r_K in radius given by Kelvin's relation [2]

$$r_K = \frac{2\gamma M}{\rho RT \ln(Ps/P)} \tag{1}$$

P is the water-vapor pressure, Ps the water vapor pressure at saturation, γ the surface tension, R the universal gas constant, T the temperature in Kelvin, and ρ and M are respectively the density and molecular weight of water. Since capillary condensation enhances the sensing capabilities of a material, pore size distribution has been widely considered to be an important parameter in determining the sensitivity in a particular humidity range [32,41]. As suggested by Shimizu et al [32], considerable effort has focused on fabricating alumina with containing a wide pore size distribution to realize a humidity sensor capable of operating over a wide range of humidity. However the ability to reproduce a specific wide range of pore size distributions, 0.1 nm to 100 nm as suggested [32], is at best a difficult task. The results of our study on uniform nanoporous alumina films made through anodization show that an easily built and highly reproducible wide range humidity, and ammonia, sensor can be achieved using nano-dimensional pores of a narrow size distribution. It should be noted that we found the Al_2O_3 sensors unresponsive to carbon dioxide.

The gas sensing characteristics of a given sensing element depend upon the material used, the method of preparation, and the resulting microstructure. In the present study alumina films were formed by anodizing aluminum thick films protected on the back side by an adhesive layer. The anodization technique used [42-44] creates self-organized alumina pore arrays from the aluminum starting material. To understand the underlying physical sensing mechanisms we employed impedance spectroscopy [45] to characterize the sensors, a powerful non-destructive technique that represents microscopic physiochemical processes occurring in the material through their electrical equivalent circuits.

Experimental

Sample preparation

Adhesive-backed aluminum tape (99% pure) purchased from Tesa Tape Inc. [46] was used for anodization. A platinum electrode served as the cathode. The electrodes were separated a distance of 2 cm. Samples SO50, SO30, and DS15 were prepared under the conditions given in Table I. Per sample notation, the first letter denotes a single S or double D step anodization process; the second letter denotes the use of sulfuric S or oxalic O acid in the anodization bath; the two digit number denotes the anodization voltage.

Table 1. Anodization conditions used for making nanoporous alumina films.

Sample	Electrolyte (amount in water)	Anodizing voltage	Duration of anodization (min.)	No. of anodization stages
SO50	2 wt% oxalic acid	50V	120	one
SO30	2 wt% oxalic acid	30V	120	one
DS15	4 wt% sulfuric acid	15V	120	two

It was observed that single step anodization results in disordered pore structures at low voltages. Hence a double step process was used for making sample DS15. These samples were initially anodized using the conditions given in Table I. The samples were then immersed in an aqueous solution containing 1.8 wt% chromic acid and 4 wt% phosphoric acid for 12 hours to remove the initial nanoporous layer while keeping the non-porous bottom layer of alumina intact. The samples were rinsed in distilled water, and again anodized under the same conditions used for the first anodization step.

Immediately after anodization all samples were thoroughly washed in distilled water and then dried in a nitrogen atmosphere at 100°C. The final dimension of the sensor was approximately 2 cm $\times$ 2 cm; an interdigital capacitor pattern of dimension 1.2 cm $\times$ 1.2 cm was formed on the surface of the alumina films by evaporating gold (thickness $\approx$ 250 nm) through a mask. A digital camera image of a typical sensor is shown in Figure 1.

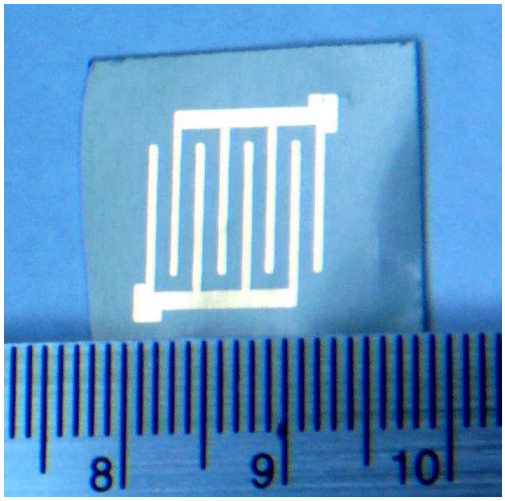

Figure 1. Digital image of a typical nanoporous alumina sensor.

Experimental set up

Sensing experiments were conducted within a sealed 60 cm^3 Plexiglas chamber. A schematic diagram of the experimental set up is shown in Figure 2. Mass flow controllers (MFC) were used for controlling and monitoring the flow. For creating the necessary humidity ambient, argon passing through one MFC was bubbled through a bottle containing de-ionized water and then mixed with dry argon coming from another MFC in appropriate ratios before passing through to the test chamber. The total flow was maintained at 500 sccm. Chamber humidity was monitored using the humidity probe of a Keithley 6517A electrometer. For ammonia sensing argon and ammonia were mixed in different ratios while keeping the total flow constant at 500 sccm; the purity of the ammonia gas was 99.99%.

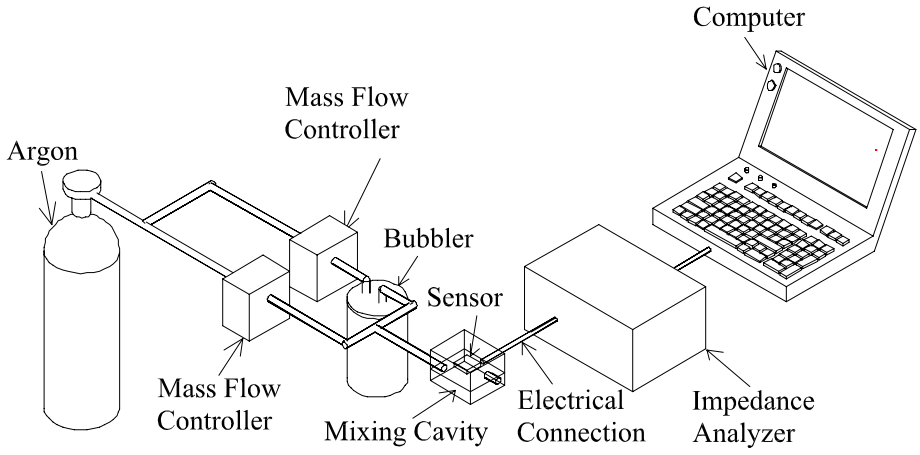

Figure 2. Schematic diagram of the experimental set up.

Sensor impedance was measured over the frequency range 5 Hz to 13 MHz using a computer controlled Hewlett Packard impedance analyzer (4192A) fitted with a test fixture (Agilent 16034E). A signal amplitude of 90 mV was used for all measurements. Electrical contact was made between the

sensor and the impedance analyzer test fixture by 42 gauge 5 cm long jumpers, adhered to the interdigital electrodes using silver paste. The contacts were subsequently annealed at 100°C for two hours to cure the silver paste. All measurements, except where noted, were carried out at room temperature (23°C).

Results and Discussion

Surface morphology

The surface morphology of the anodized alumina samples was studied using a Hitachi S-900 field emission scanning electron microscope (FESEM). Figures 3 through 5 show FESEM images of, respectively, samples SO50, SO30, and DS15 and their corresponding estimates of pore size distribution. Samples SO50, SO30, and DS15 have, respectively, average pore diameters of 45.2 nm, 38.4 nm, 13.6 nm, corresponding standard deviations of 3.4 nm, 7.8 nm, and 2.6 nm. All samples have predominantly ordered pore structures.

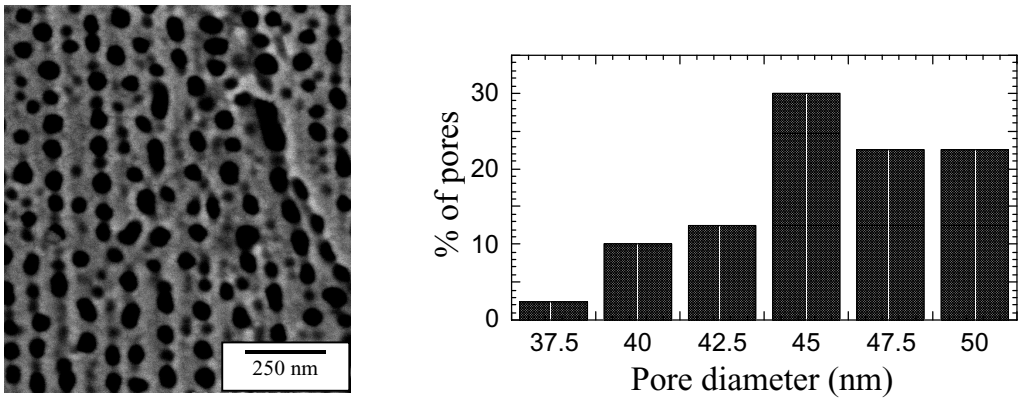

Figure 3. Field emission scanning electron microscope (FESEM) image of sensor SO50 with corresponding pore size distribution.

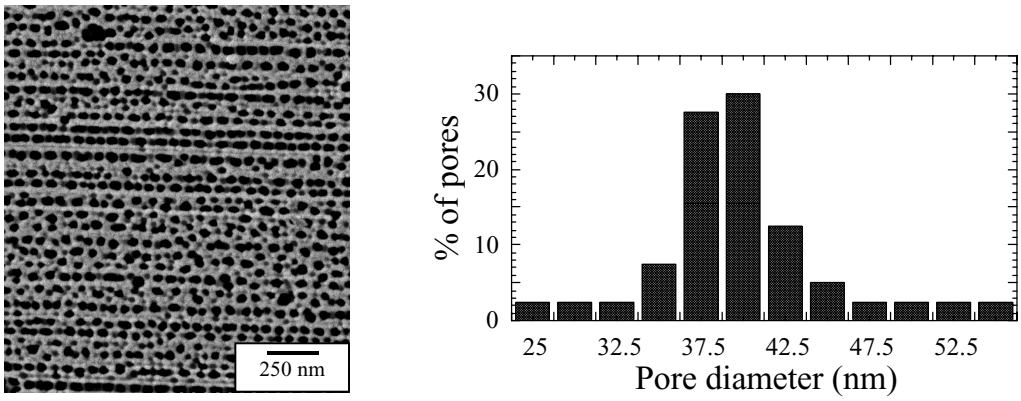

Figure 4. Field emission scanning electron microscope (FESEM) image of sensor SO30 with corresponding pore size distribution.

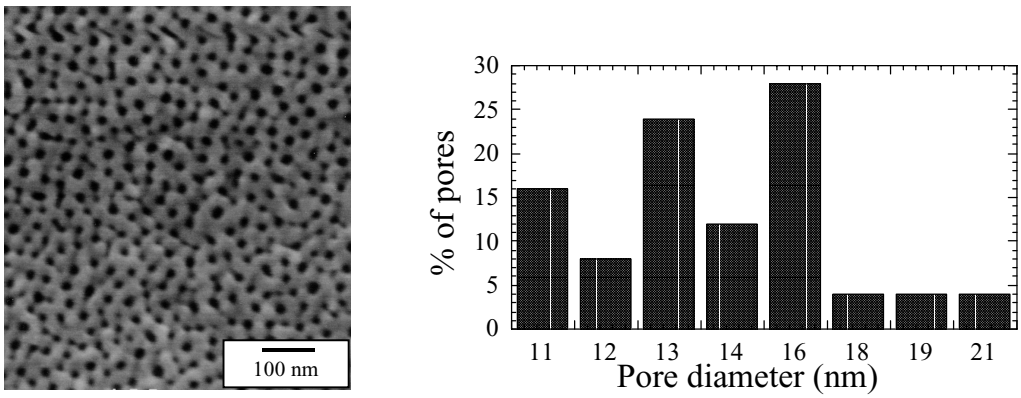

Figure 5. Field emission scanning electron microscope (FESEM) image of sensor DS15 with corresponding pore size distribution.

Humidity Sensing

Figure 6 shows the measured 5 kHz sensor impedance of the different sensors with respect to humidity. Sensor DS15 is sensitive to a wide range of humidity levels, approximately 20% to 90% RH, with an impedance variation of approximately three orders of magnitude. Sensors SO30 and SO50 become sensitive to humidity at relatively high humidity levels, approximately 65 % and 75% RH respectively. It is clear from Figure 6 that smaller pore sizes increase the range of humidity values over which the sensor is responsive, and increases the sensitivity at lower humidity levels. Therefore optimal pore size can be selected for the operating region of interest.

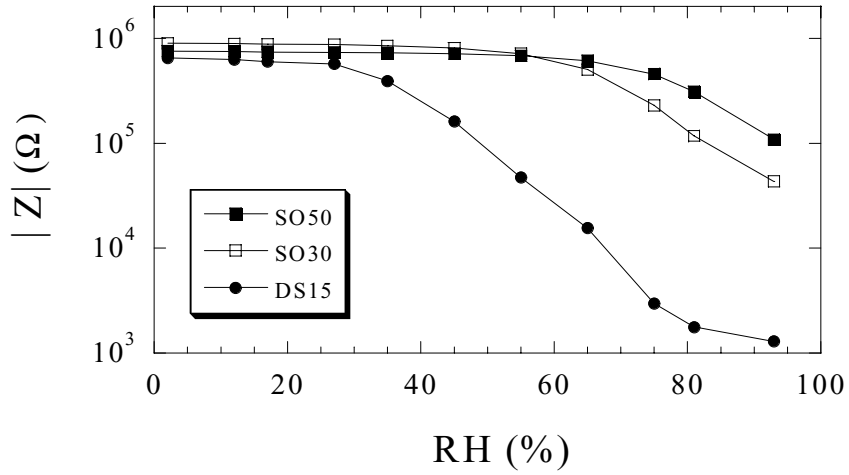

Figure 6. Impedance of sensors measured at 5 kHz over different humidity levels.

The effect of measurement frequency on the humidity sensitive regime of the sensors was also investigated. Figure 7 shows the response of sensor DS15 to humidity at different measurement frequencies. It can be seen from the figure that as frequency decreases the width of the sensitive region increases, and the point at which the sensor becomes responsive shifts to lower relative humidity

values. For a given pore size, the humidity sensitive region of operation can be selected by frequency tuning.

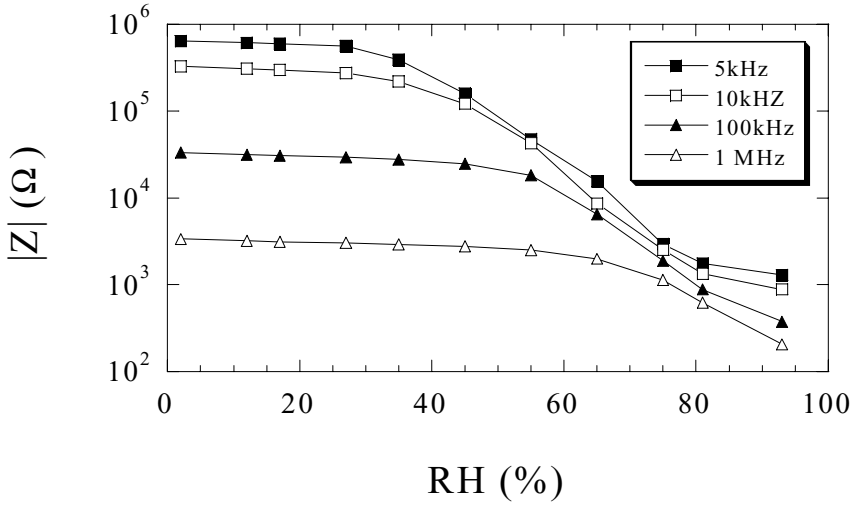

Figure 7. Variation of sensor DS15 impedance with humidity and measurement frequency.

The response time, defined as the time needed to reach 90% of the final signal for a given relative humidity, and recovery time defined as the time taken for the signal to come to within 10% of the initial value, were determined by alternately exposing the sensors to a 2% or 45% RH ambient with impedance measured at 5 kHz. The response time and recovery times corresponding to different pore diameters are shown in Figure 8, which indicates that the response time decreases with increasing pore size. The minimum response/recovery times were observed for SO50, the sample with the largest pore size. A typical response/recovery graph of sample SO50 is shown in the inset of Figure 8. It was observed that all sensors were completely reversible, regaining their original impedance values even after repeated exposure to high humidity levels.

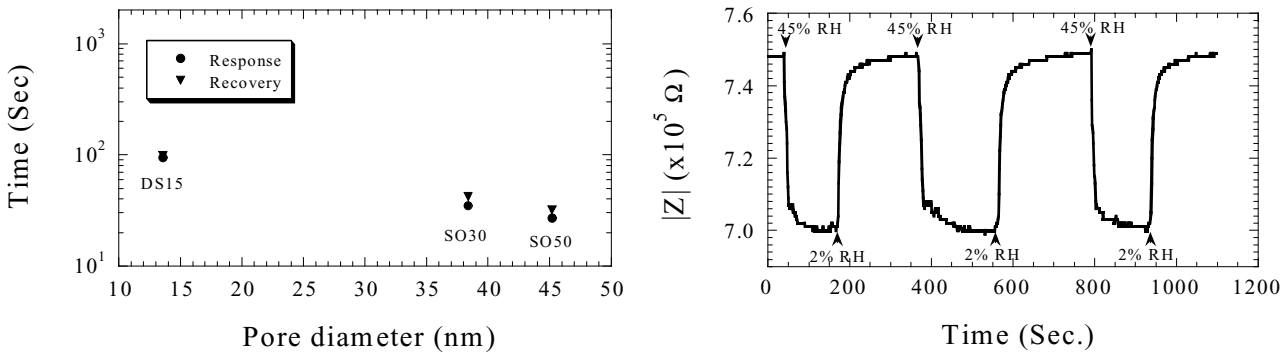

Figure 8. (Left) Dependence of response time and recovery time on pore size. (Right) The response of the sensor SO50 on repeated exposure to a humidity level of 45%.

The impedance spectra of the sensors were taken over a range of humidity levels. The total impedance was resolved into real (Z') and imaginary (Z'') parts and Cole-Cole impedance plots

constructed. Figures 9 through 11 show, respectively, the Cole-Cole plot of sensors SO50, SO30, and DS15. The two equivalent circuit models shown in Figure 12 were used for fitting the experimental data. The fitting was accomplished using the complex nonlinear least square-fitting program, LEVM, provided by J.R. Macdonald and Solartron Analytical [47]. The dots in the plots represent experimental data, and lines the equivalent circuit model fit. The equivalent circuit, denoted (a) or (b) with reference to Figure 12, used for fitting is denoted near the corresponding curves in Figures 9-11. It is clear from the figures that the equivalent circuit models closely fit the experimental data. It may be noted that these equivalent circuit models are different from the empirical model suggested by Falk et al [48] for porous alumina sensors fabricated by anodizing aluminum thin films. In the equivalent circuit models R_1 and R_2 represent two frequency independent resistors in parallel with dispersive frequency dependent capacitors, $C_{n1}(\omega)$ and $C_{n2}(\omega)$ respectively [49]. These non-Debye capacitances can be expressed in a general form as $C_n(\omega) = B_n(i\omega)^{n-1}$ where B_n is a constant for a given set of experimental conditions and n takes the value between 0 and 1 according to the local microscopic environment through which charge transport takes place [13,49,50]. B_n behaves as an ideal frequency independent capacitor as n approaches 1, and an ideal conductance when the value of n approaches 0 [45].

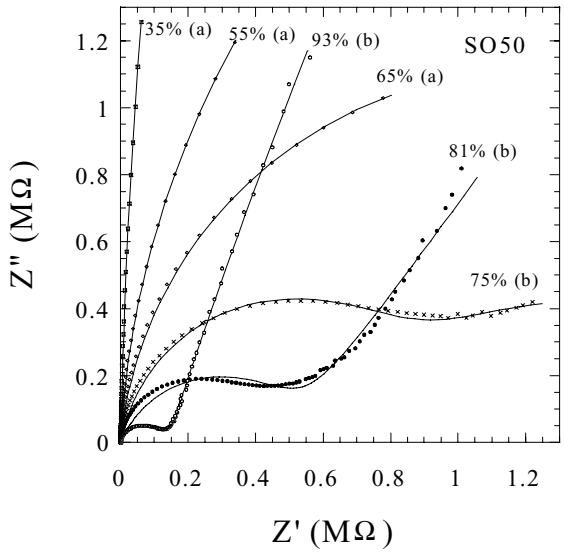

Figure 9. Cole-Cole plot of sensor SO50 as a function of humidity. The points represent the experimental data and lines the fit with the equivalent circuit model given in Figure 12. The RH values at which the data was collected and the equivalent circuit used for fitting each curve (given as (a) or (b) denoting the circuit of Figure 12a and 12b respectively) are shown adjacent to each curve.

On examining Figure 9, it can be seen that at low humidity levels the Cole-Cole plot describes an arc having a very large radius of curvature. As humidity increases, the radius reduces and at an RH of about 80% the complete semicircle comes inside the measurable impedance range. However at the same humidity level a spur appears in the low frequency region that distorts the semicircle. The spur, which can be viewed as part of a second semicircle, dominates at higher humidity levels while the semicircle described by the high frequency impedance values diminishes in size. For sensors SO50,

SO30 and DS15 the RH at which the high frequency semicircle comes completely within the measurable impedance range is, respectively, ≈ 75%, 65% and 30%; these values roughly match the points of inflection seen in Figure 6.

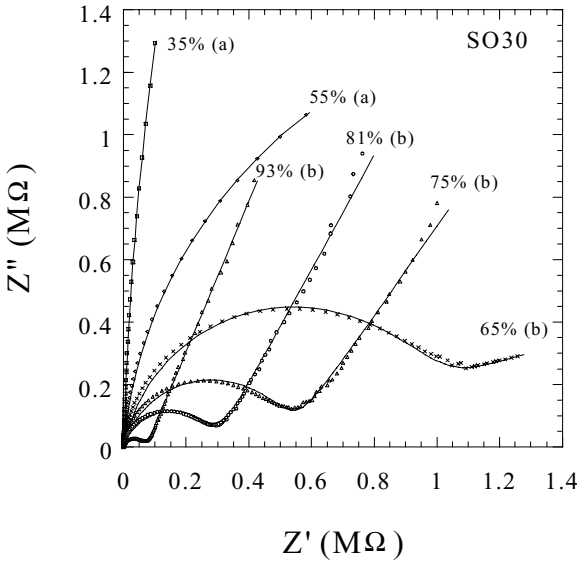

Figure 10. Cole-Cole plot of sensor SO30 at different humidity levels. The points represent the experimental data and lines the fit with the equivalent circuit model given in Figure 12. The RH values at which the data was collected and the equivalent circuit used for fitting each curve (given as (a) or (b) denoting the circuit of Figure 12a and 12b respectively) are shown adjacent to each curve.

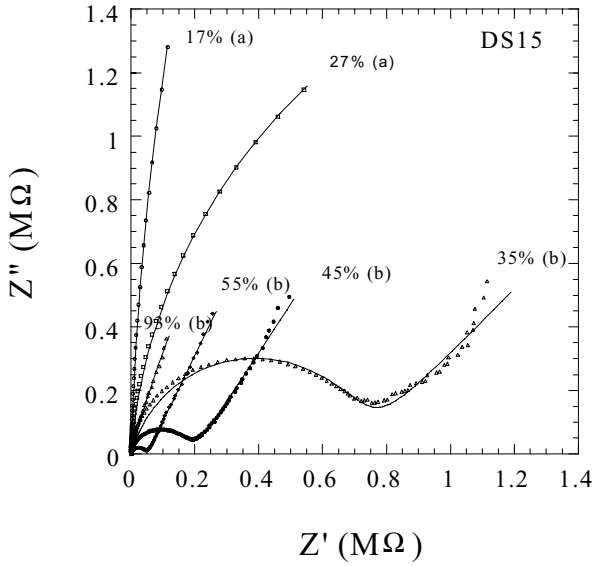

Figure 11. Cole-Cole plot of sensor DS15 at different humidity levels. The points represent the experimental data and lines the fit with the equivalent circuit model given in Figure 12. The RH values at which the data was collected and the equivalent circuit used for fitting each curve (given as (a) or (b) denoting the circuit of Figure 12a and 12b respectively) are shown adjacent to each curve.

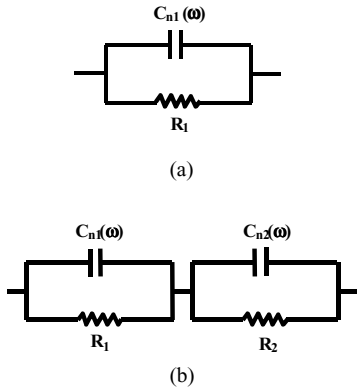

Figure 12. Equivalent circuits used for fitting the experimental data. The circuit in (a) was used when only high frequency semicircle was present and that in (b) was used where the low frequency spur co-exists with the high frequency semicircle.

The fundamental mechanism that enables ceramic sensors to sense humidity is the physisorption of water molecules on an initially chemisorbed layer of hydroxyl ions [3,51]. The chemisorbed hydroxyl ions enhance the electrical conductivity of the sensor either by donating electrons to the conduction band of the base material or through proton hopping between adjacent hydroxyl groups upon application of an electric field. The process of chemisorption occurs at very low humidity levels, and is unaffected by further changes in humidity. However an increase in humidity makes the water molecules physisorb onto this hydroxyl layer. The effectiveness of physisorption depends upon the cation charge complexes (from the material or the impurities), and the hydroxyl ions (water molecules present at the surface of the base material) [43]. The physisorption process is facilitated by higher surface charge densities. During formation of the first physisorbed layer, a water molecule attaches to two neighboring hydroxyl groups through hydrogen double bonds and a proton may be transferred from a hydroxyl group to the water molecule to form an H_3O^+ ion.

When the physisorption occurs within less than a mono layer, i.e. when clusters of physisorbed molecules are present at the surface, it is thought H_3O^+ diffusion within hydroxyl groups and proton transfer between adjacent water molecules clusters takes place [43]. However Khanna and Nahar [44-46] refute this theory. They argue that the proton diffusion is less probable in a surface that contains hydroxyl ions and clusters of physisorbed molecules, and hence cannot account for the conductivity of porous alumina at an RH less than 40%, i.e. before the first monolayer is formed. Instead they suggested a phonon-assisted electron tunneling mechanism at low humidity levels in which electron tunneling occurs from one water molecule to another as enhanced by the surface anions of the alumina sensors.

At higher humidity levels, the number of physisorbed layers increases allowing each water molecule to be singly bonded to a hydroxyl group, and proton hopping between adjacent water molecules in the continuous water layer takes place. The conduction process is the same as that of pure water and is called Grotthuss chain reaction [43]. The dominant charge carrier in a high humidity environment is therefore the H+ ions (protons). The concentration of H+ increases with increasing humidity and H+ move freely through the water-like layer. As per the theory of Khanna and Nahar [44], in porous alumina the protons for conduction are donated not only by H_2O, but also by the

$Al(OH)_3$ formed as a result of water adsorption and the impurity anion incorporated in the film from the electrolyte during anodization [47-49]. The water-like network consists of singly bonded water molecules which possess a high dielectric constant as they form dipoles and reorient freely under an externally applied electric field. The impedance of the nanoporous alumina sensors contain this capacitive contribution as well.

In porous ceramics, in addition to the above discussed processes, capillary condensation according to Equation (1) also takes place. Capillary condensed water reduces the impedance of the sensor drastically.

On analyzing Figures 9-11, the high frequency semicircle that diminishes in size with increasing RH arises due to the effect of a physisorbed water layer at the surface. Therefore R_1 in the equivalent circuit of Figure 12 represents the charge transfer resistance through the adsorbed water layer. The effect of electronic conduction through the alumina bulk is parallel to that of the surface conduction affected by the adsorbed water layer. This bulk conduction process is dominant only at extremely low humidity values when there are only a few adsorbed molecules. Hence the incomplete semicircle, or arc, in the low humidity region is partially determined from the base alumina. B_{n1} represents the capacitance contribution from the adsorbed water layer. The large spurs seen in the low frequency region is a consequence of ion migration in the adsorbed layer towards electrodes [37,41]. This migration leads to accumulation of ions (space charge formation) at the electrodes. Since the relaxation time of ion migration is larger than the charge transfer process it is seen only at low frequencies. The accumulated ions in the adsorbed water layer give rise to R_2 and B_{n2}.

From the equivalent circuits given in Figure 12, it can be seen that the presence of ion accumulation represented by the combination of R_2 and $C_{n2}(\omega)$ increases the overall impedance of the sensor. Hence the reduction in impedance caused at high humidity due to charge transfer process is countered by ion accumulation.

To better understand the fundamental sensing mechanisms, R_1 obtained through the numerical fitting program for the different sensors is plotted in Figure 13. It can be seen from Figure 13 that R_1, which is the resistance to charge transport in a static electric field by the material containing an adsorbed water layer in the absence of ion migration, is linear with RH in a semi-log plot. For sensor DS15, R_1 decreases to a few hundred ohms at high RH levels indicating that the observed conductivity is not merely because of the protons provided by the adsorbed water layer. Since de-ionized water and argon gas are used for creating the required humidity environment it is reasonable to assume that the surface of the alumina films contain anions, presumably from the electrolyte used for anodization, that controls conduction through the adsorbed layer [48].

In light of the above observations we propose the following model to explain the behavior of nanoporous alumina in response to humidity. The anodization process results in a certain amount of electrolyte anions trapped within the pores [44,47,48]. Even in a low humidity regime the presence of these anions on the sensor surface provides a high charge density for easy physisorption of water molecules. The result is formation of a liquid-like network within the pores. The impurity anions also act as proton donors by a dissociative mechanism [44], joining the protons donated by the water molecules. The smaller the pore size the lower the RH level at which the liquid-like network is formed.

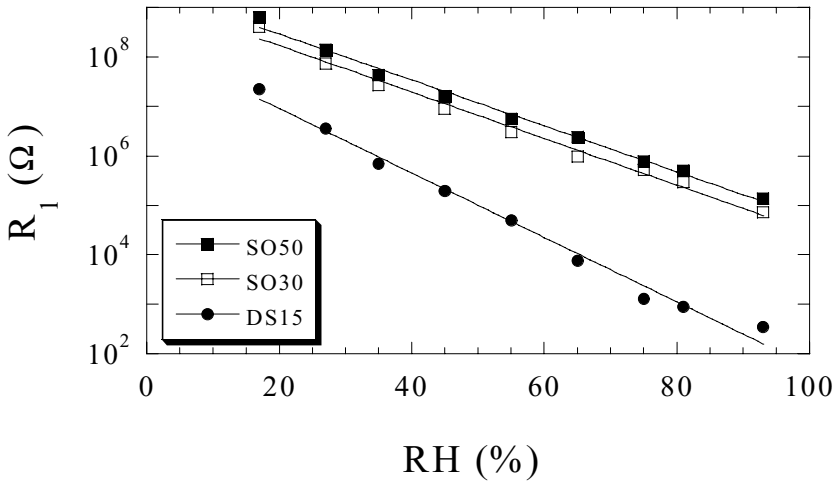

Figure 13. Humidity dependence of resistance R_1 of different sensors obtained by fitting the equivalent circuit model (Figure 12a) with experimental data.

For samples SO50 and SO30, the liquid network formation occurs only at higher humidity levels. Though Khanna and Nahar suggested [44] a liquid network formation above 40% RH, our studies showed this can occur at humidity levels less than 27%, a consequence of the nano-dimensional pores containing impurity anions. After the formation of the liquid-like network, the ions migrate easily towards the electrode and accumulate there. Although this ion migration is dominated by protons since they are the majority carriers, impurity anions adsorbed on the film surface may also take part in the migration process at low frequencies in a manner similar to impurity ion movement in water.

For small pore size sensors, the first semicircle is highly distorted by the low frequency spur originating with ion migration. A relatively large number of mobile ions might be present in these sensors leading to an enhanced accumulation of protons at the electrode-sample contact. As mentioned earlier, the dipoles in the singly bonded adsorbed water layer are free to rotate in an electric field. Hence in the region close to the electrode-alumina interface, the adsorbed water layer exhibits a net dipolar orientation and, therefore, it does not display its normal dielectric constant [37,41]. Depending on ion size up to a monolayer of charge can exist at the electrode [37]; the diffuse (Gouy) layer of counter ions spreads away from this inner (Stern) layer. The number of ions available for forming the Stern and Gouy layers at a particular frequency increases with increasing number of physisorbed layers. Hence as the number of physisorbed layers increases, the Stern and Gouy layers start forming at higher frequencies.

In summary, at high frequencies the charge transfer process dominates the impedance mechanism, which appears as a semicircle in the Cole-Cole plot. At lower frequencies mass transport takes place and its contribution to impedance distorts the semicircle. At very low frequencies the effects of mass transport appear, which results in the spur on the impedance plot, completely dominating the effect of charge transfer processes. The effect of charge transfer in the adsorbed water, which acts to decrease the sensor impedance, competes with ion accumulation which increases the measured impedance.

The response and recovery behavior seen in Figure 8 shows that sensors with smaller pore sizes require longer periods of time for diffusion of the water molecules.

With reference to Figure 7, the relative humidity level at which the sharp decrease in impedance occurs shifts higher with increasing frequency. This result can be explained using the equivalent circuit shown in Figure 12a, i.e. the circuit in the absence of ion accumulation. At high frequencies the reactive impedance X_c of $C_{n1}(\omega)$, equal to $X_c = 1/j\omega C_{n1}(\omega)$, is low and hence impedance is largely determined by R_1. As humidity increases R_1 decreases, however this translates into a reduction in impedance only at relatively low frequencies where the value of R_1 is comparable to or less than the capacitive reactance of $C_{n1}(\omega)$. As the measurement frequency is reduced the reactance of $C_{n1}(\omega)$ decreases, hence the effect of R_1 becomes more significant at lower humidity levels.

Ammonia Sensing

The response of sensors DS15, SO50, and SO30 to ammonia gas was investigated at a measurement frequency of 5kHz. Argon and ammonia were mixed in different ratios while keeping the total flow constant at 500sccm. Figure 14 shows the response of sensor DS15, impedance magnitude and phase, with changing ammonia concentration, Figure15 DS30, and Figure 16 DS50. After each exposure to ammonia gas the sensor was brought to its original condition by passing 100% argon. The time interval between switching of the argon to argon-ammonia mixture, or vice-versa, was fixed for a particular sensor. The ammonia concentration was increased in discrete steps to 100% and then decreased to 0% in the same manner.

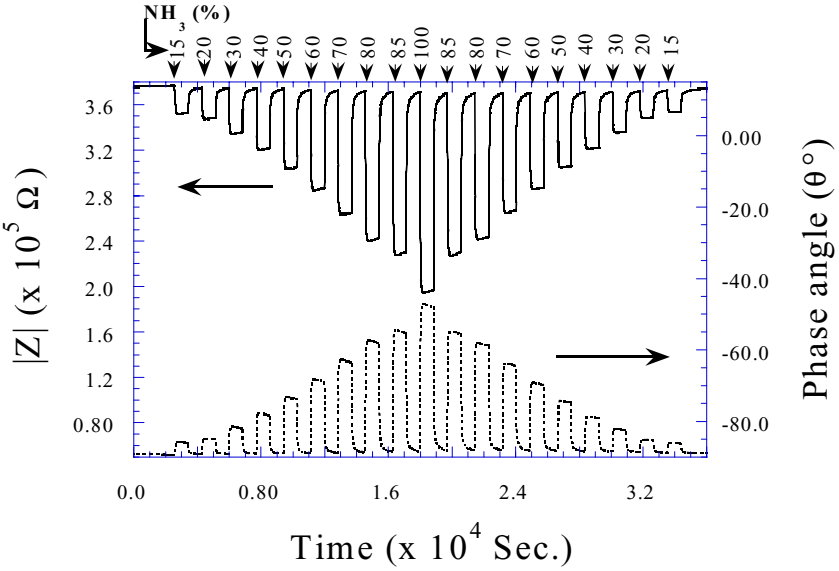

Figure 14. Change in impedance magnitude and phase of sensor DS15 in response to changing ammonia concentration. Argon is used as the carrier gas. The sensor response is completely reversible.

The ammonia sensitivity of each sensor is determined using the formula

$$\text{Sensitivity} = \frac{Z_{\text{arg on}} - Z_{\text{ammonia}}}{Z_{\text{arg on}}} \times 100\% \qquad (2)$$

Z_{argon} is the measured impedance in the presence of pure argon, and $Z_{ammonia}$ the measured impedance in the presence of the argon-ammonia mixture. Maximum sensitivity is achieved with the sensor of minimum pore size, DS15. As seen in Figure 17 increasing pore size reduces ammonia sensitivity. The effect of temperature on ammonia measurement sensitivity was also investigated. As seen in Figure 17 the sensitivity of SO30 is dramatically decreased with an increase in temperature to 40°C; similar results were found for the other sensors.

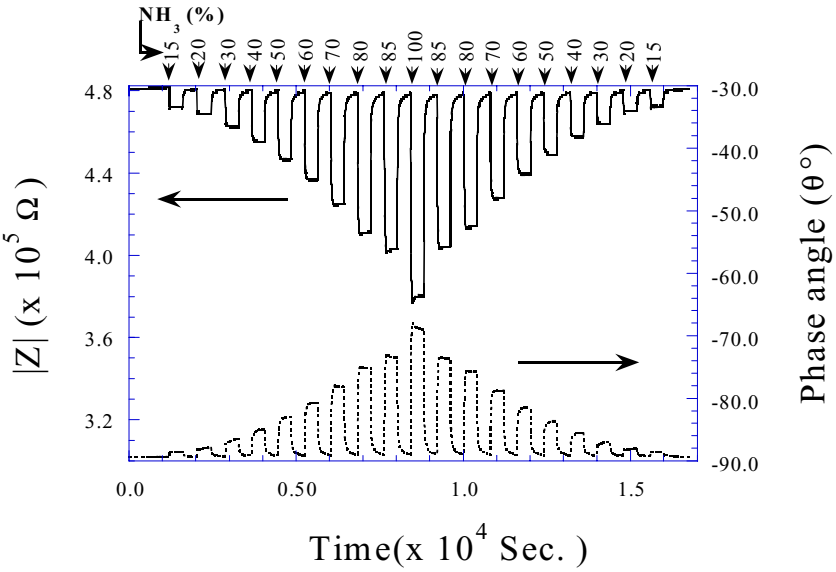

Figure 15. Change in impedance magnitude and phase of sensor SO30 in response to changing ammonia concentration. Argon is used as the carrier gas. The sensor response is completely reversible.

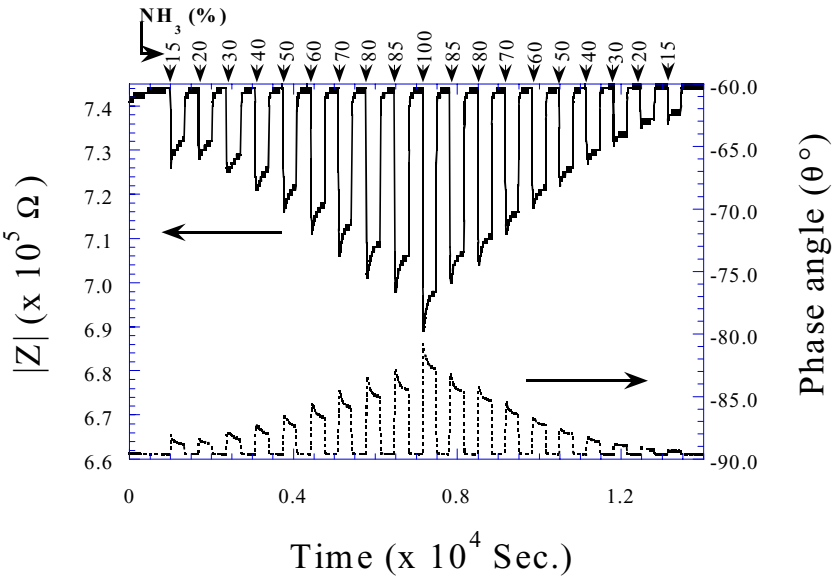

Figure 16. Change in impedance magnitude and phase of sensor SO50 in response to changing ammonia concentration. Argon is used as the carrier gas. The sensor response is completely reversible.

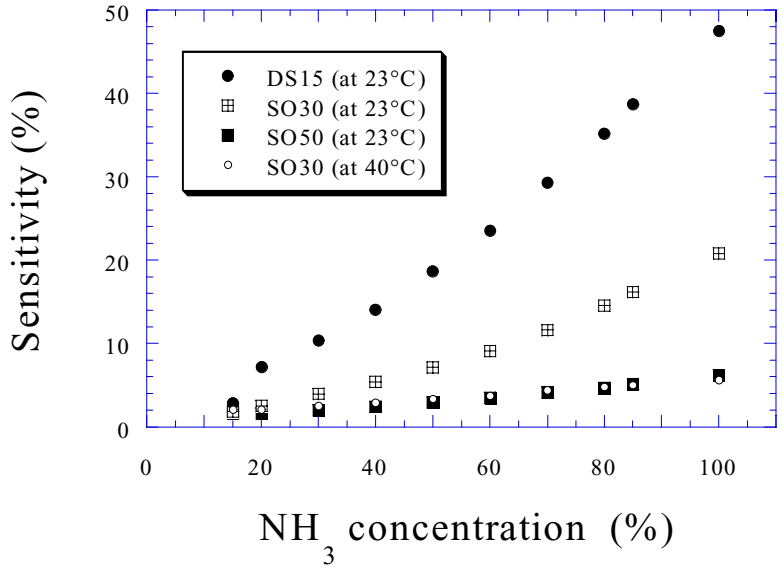

Figure 17. Ammonia sensitivity as a function of pore size and temperature.

The rapid drop in sensitivity with temperature suggests that the ammonia molecules are loosely bonded to the alumina surface. Hence it appears that physisorption is responsible for the sensing action. It is not clear whether the presence of ammonia simply increases the dielectric constant of the sensor, or whether it also facilitates ionic current conduction through the surface. As discussed earlier, both these factors are responsible for the humidity sensitivity of alumina.

The response times of the sensors for different ammonia concentrations are shown in Figure 18, with recovery times shown in Figure 19. Not surprisingly, the response and recovery times are largest for the smallest pore size sensor, DS15, as smaller pores increase the time required for molecules to diffuse into and out of the sensor interior.

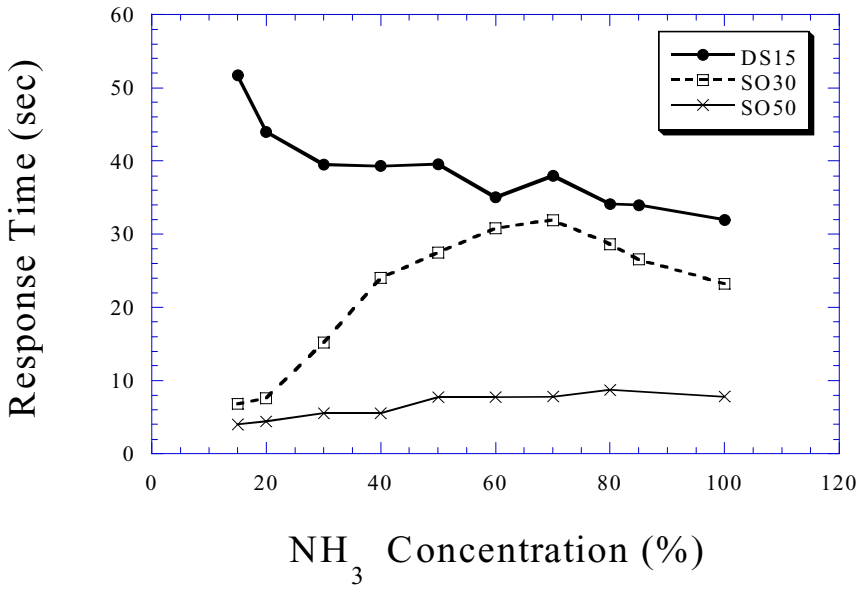

Figure 18. Sensor response times to changing ammonia concentrations.

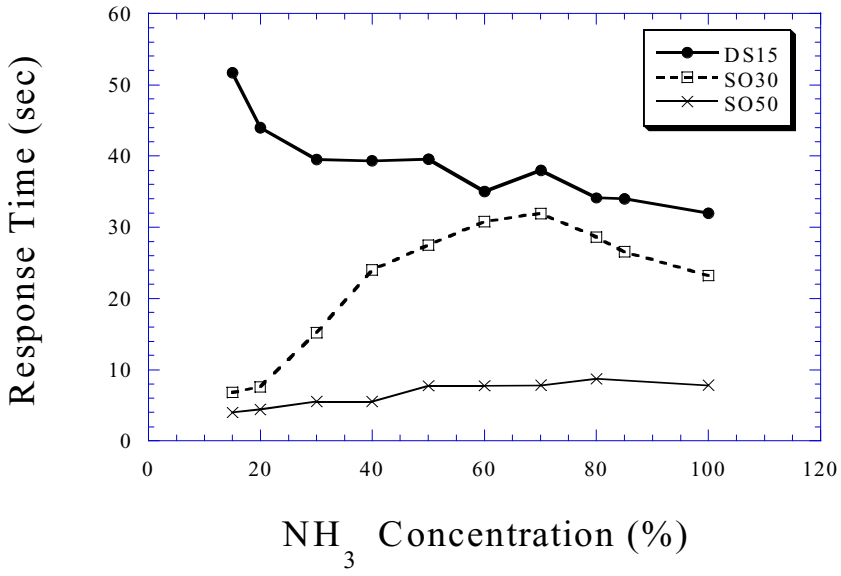

Figure 19. Sensor recovery times changing from an ammonia environment to an argon environment.

The response and recovery times of DS15 decrease with increasing ammonia concentration. The results indicate that with increasing ammonia concentration (partial pressure of ammonia) more molecules are pressurized to rapidly reach the pore interior, where they are weakly attached to the alumina surface molecules, or previously adsorbed ammonia molecules. Similarly, with decreasing partial pressure of ammonia the molecules easily break the bonds and diffuse out of the pores. The influence of the pores on the sensitivity of SO30 is considerably less than that seen for DS15; a decrease in response and recovery times can be seen only at high ammonia concentration. For SO50 pore diffusion plays essentially no role in determining sensor behavior, with no reduction in response or recovery times seen even at high ammonia concentrations.

Conclusions

Nanoporous alumina sensors fabricated by anodization of adhesive-backed aluminum tape exhibit pore size and frequency dependent humidity and ammonia sensing characteristics. Sensors over a range of uniform pore size, from approximately 45 nm to 13 nm diameter, were studied. Sensor DS15, with a 13.6 nm pore size, standard deviation $\approx$ 2.6 nm, exhibited qualities desirable for a high performance humidity sensor. It demonstrated more than three orders of magnitude variation in measured impedance over a RH range of ~20% to ~90%, with a response time of ~95 sec.

The mechanism responsible for the sensing action of the nanoporous alumina sensors was studied by representing the impedance spectra at different humidity levels in Cole-Cole plots. This enables the competing impedance determining processes occurring in the sensors to be identified, namely charge transfer and mass transport through the physisorbed water layer, as dependent upon the humidity level and input signal frequency. Charge transfer was found to enhance the sensitivity by causing a large variation in impedance (evident from the variation of R_1 in Figure 13) with respect to humidity. Mass

transport leads to accumulation of ions at the electrodes that tends to decrease the measurement sensitivity by increasing the impedance. Hence a proper choice of operating frequency, high enough to avoid ion accumulation, is essential for the optimum sensor performance.

It has been inferred from our results that anions become incorporated into the alumina film during the anodization process, supporting the hypothesis of Khanna and Nahar [44-46], where they act as proton donors and facilitate the adsorption of water molecules. Hence liquid-like charge transfer networks are formed at relatively lower humidity levels for the smaller pore sized sensors. This process, rather than capillary condensation, is primarily responsible for the observed humidity sensing behavior of the sensors. Our studies show that a distribution of pore sizes, as suggested by Shimizu et al [32], is not necessary to obtain sensitive performance over a wide humidity range. As demonstrated herein, such optimal performance can be obtained with uniform nano-dimensional pores containing adsorbed anionic impurities.

The use of alumina for room temperature (23°C) sensing of ammonia is demonstrated, with all sensors showing a completely reversible response upon changing ammonia partial pressures. Higher operating temperatures dramatically reduce sensor sensitivity, indicating that the ammonia molecules are weakly attached to the alumina molecules. The results indicate that physisorption is responsible for the sensing action. Pore sizes of 50 nm or greater do not limit ammonia diffusion, with the response and recovery rates of such sensors independent of ammonia concentrations.

Acknowledgements

This work was supported by the National Science Foundation under contracts NSF DMR–9976851, ECS–9988598, and ECS–9875104.

References

1. Kulwicki, B. M. Humidity sensors. *Journal of American Ceramic Society* **1991**, *74*, 697-708.
2. Arai, H.; Seiyama, T. Humidity Sensors, in Sensors: a comprehensive survey, W. Gopel, J. Hesse and J.N. Zemel (Eds.), VCH, Weinheim, Vol. 3, (1992) pp. 981-1012.
3. Traversa, E. Ceramic sensors for humidity detection: the state-of-the-art and future developments. *Sensors and Actuators B* **1995**, *23*, 135-156.
4. Yamazoe, N.; Shimizu, Y. Humidity sensors: Principles and applications. *Sensors and Actuators* **1986**, *10*, 379-398.
5. Bearzotti, I.; Fratoddi, L.; Palummo, S.; Petrocco, A.; Furlani, C.; Sterzo, Lo,; Russo, M.V. Highly ethynylated polymers: synthesis and applications for humidity sensors. *Sensors and Actuators B* **2001**, *76*, 316-321
6. Sakai, Y.; Sadaoka Y.; Matsuguchi, M. Humidity sensors based on polymer thin films. *Sensors and Actuators B* **1996**, *35*, 85-90
7. Grimes, C.A.; Kouzoudis, D. Remote Query Measurement of Pressure, Fluid-Flow Velocity, and Humidity Using Magnetoelastic Thick-Film Sensors. *Sensors and Actuators A* **2000**, *84*, 205-212.

8. Ong, K.G.; Grimes, C.A.; Robbins, C.L.; Singh, R. S. Design and Application of a Wireless, Passive, Resonant-Circuit Environmental Monitoring Sensor. *Sensors and Actuators A* **2001**, *93*, 33-43.
9. Seiyama, T.; Yamazoe, N.; Arai, H. Ceramic humidity sensors. *Sensors and Actuators* **1983**, *4*, 85-96.
10. Ketron, L. Ceramic sensors. *Ceramic Bulletin* **1989**, *68*, 860-865
11. Traversa, E.; Gusmano, G.: Montenero, A. Innovative humidity sensitive electrical properties of sol-gel processed ceramic thin films. *European Journal of Solid State Inorganic Chemistry* 1995, *32*, 719-729.
12. Jain, M.K.; Bhatnagar, M.C.; Sharma, G.L. Effect of Li^+ doping on ZrO_2-TiO_2 humidity sensor. *Sensors and Actuators B* **1999**, *55*, 180-185
13. Varghese, O.K.; Malhotra, L.K. Studies of ambient dependent electrical behavior of nano-crystalline SnO_2 thin films using impedance spectroscopy. *Journal of applied physics* **2000**, *87*, 7457-7465.
14. Sberveglieri, G.; Murri, R.; Pinto, N. Characterization of porous Al_2O_3-SiO_2/Si sensor for low and medium ranges. *Sensors and Actuators B* **1995**, *23*, 177-180.
15. Traversa, E.; Baroncini, M.; Bartolomeo, E. D.; Gusmano, G.; Innocenzi, P.; Martucci, A.; Bearzotti, A. Electrical humidity response of sol-gel processed undoped and alkali doped TiO_2-Al_2O_3 thin films. *Journal of the European Ceramic Society* **1999**, *19*, 753-758.
16. Chou, K.-S.; Lee, T.-K.; Liu, F.-J. Sensing mechanism of a porous ceramic as humidity sensor. *Sensors and Actuators B* **1999**, *56*, 106-111.
17. Traversa, E.; Gnappi, G.; Montenero, A.; Gusmano, G. Ceramic thin films by sol-gel processing as novel materials for integrated humidity sensors. *Sensors and Actuators B* **1996**, *31*, 59-70.
18. Yeh, Y.-C.; Tseng, T.-Y.; Chang, D.-A. Electrical properties of porous titania ceramic humidity sensors. *Journal of the American Ceramic Society* **1989**, *72*, 1472-1475.
19. Traversa, E. Design of ceramic materials for chemical sensors with novel properties. *Journal of American Ceramic Society* **1995**, *78*, 2625-2632.
20. Yamamoto, T.; Murukami, K. Humidity sensor using TiO_2-SnO_2 ceramics, in Chemical Sensor Technology, T. Seiyama (Ed.), vol.2, (1989) pp. 133-149.
21. Ansbacher, F.; Jason, A. C. Effects of water vapour on the electrical properties of anodised aluminum. *Nature* **1953**, *171*, 177-178.
22. Khanna, V. K.: Nahar, R. K. Effect of moisture on the dielectric properties of porous alumina films. *Sensors and Actuators* **1984**, *5*, 187-198.
23. Basu, S.; Chatterjee, S.; Saha, M.; Bhandyopadhay, S.; Mistry, K. K.; Sengupta, K. Study of electrical characeristics of porous alumina sensors for detection of low moisture in gases. *Sensors and Actuators B* **2001**, *79*, 182-186
24. Sberveglieri, G.; Anchisini, R.; Murri, R.; Ercoli, C.; Pinto, N. An Al_2O_3 sensor for low humidity content: characterisation by impedance spectroscopy. *Sensors and Actuators B* **1996**, *32*, 1-5.
25. Mai, L. H.; Hoa, P. T. M.; Binh, N. T.; Ha, N. T. T.; An, D. K. Some investigation results of the instability of humidity sensors based on alumina and porous silicon materials. *Sensors and Actuators B* **2000**, *66*, 63-65.

26. Chatterjee, S.; Basu, S.; Bandyopadhay, S.; Mistry, K. K.; Sengupta, K. Humidity sensor using porous tape cast alumina substrate. *Review of Scientific Instruments* **2001**, *72*, 2792-2792.
27. Nahar, R. K. Study of the performance degradation of thin aluminum oxide sensor at high humidity. *Sensors and Actuators B* **2000**, *63*, 49-54.
28. Chen, Z.; Jin, M.-C.; Zhen, C. Humidity sensors with reactively evaporated Al_2O_3 films as porous dielectrics. *Sensors and Actuators* **1990**, *2*, 167-171.
29. Basu, S.; Saha, M.; Chatterjee, S.; Mistry, K. K.; Bandyopadhay, S.; Sengupta, K. Porous ceramic sensor for measurement of gas moisture in the ppm range. *Materials Letters* **2001**, *49*, 29-33.
30. Sadaoka, Y.; Sakai, Y.; Matsumoto, S. Electrical properties of anodised aluminum in a humid atmosphere. *Journal of Materials Science* **1986**, *21*, 1269-1274.
31. Seiyama, T.; Fueki, K.; Shiokawa, J.; Suzuki, S. (Eds.), Chemical Sensors, Elsevier, New York, (**1983**).
32. Shimisu, Y.; Arai, H.; Seiyama, T. Theoretical studies on the impedance-humidity characteristics of ceramic humidity sensors. *Sensors and Actuators* **1985**, *7*, 11-22
33. Nicho, M. E.; Trejo, M.; Garcia-Valenzuela, A.; Saniger, J. M.; Palacios, J.; Hu, J. Polyaniline composite coatings interrogated by a nulling optical-transmittance bridge for sensing low concentrations of ammonia gas. *Sensors and Actuators B* **2001**, *76*, 18-24.
34. Chabukswar, V. V.; Pethkar, S.; Athawale, A. A. Acrylic acid doped polyaniline as an ammonia sensor. *Sensors and Actuators B* **2001**, *77*, 657-663.
35. Raimundo, M.; Narayanaswamy, R. Simultaneous determination of relative humidity and ammonia in air employing an optical fibre sensor and artificial neural network. *Sensors and Actuators B* **2001**, *74*, 60-68.
36. Lin, C. W.; Hwang, B. J.; Lee, C. R. Sensing behaviors of the electrochemically co-deposited polypyrrole-poly(vinyl alcohol) thin film exposed to ammonia gas. *Materials Chemistry and Physics* **1999**, *58*, 114-120.
37. Teeramongkonrasmee, M. Sriyudthsak Methanol and ammonia sensing characteristics of sol-gel derived thin film gas sensor. *Sensors and Actuators B* **2000**, *66*, 256-259.
38. Wang, Y. D.; Wu, X. H.; Su, Q.; Li, Y. F.; Zhou, Z. L. Ammonia-sensing characteristics of Pt and SiO_2 doped SnO_2 materials. *Solid-State Electronics* **2001**, *45*, 347-350.
39. Zhang, T.; Shen, Y.; Zhang, R.; Liu, X. Ammonia-sensing characteristics of Pt-doped $CdSnO_3$ semiconducting ceramic sensor. *Materials Letters* **1996**, *27*, 161-164.
40. Shimizu, Y.; Okamoto, T.; Takao, Y.; Egashira, M. Desorption behavior of ammonia from TiO_2-based specimens- ammonia sensing mechanism of double-layer sensors with TiO_2-based catalyst layers. *J. Molecular Catalysis A: Chemical* **2000**, *155*, 183-191.
41. Tao, S. H.-; Tang, W. M.-; Ping, L.; Xi, Y. Porosity control of humidity-sensitive ceramics and theoretical model of humidity-sensitive characteristics. *Sensors and Actuators* **1989**, *19*, 61-70
42. Masuda, H.; Fukuda, K. Ordered metal nanohole arrayes made by a 2-step replication of honeycomb structures of anodic alumina. *Science* **1995**, *268*, 1466-1468.
43. Masuda, H.; Hasegwa, F.; Ono, S. Self-Ordering of Cell Arrangement of Anodic Porous Alumina Formed in Sulfuric Acid Solution. *Journal of the electrochemical society* **1997**, *144*, L127-L129.
44. Jessensky, O.; Muller, F.; Gosele, U. Self-organised formation of hexagonal pore arrays in anodic alumina. *Applies Physics Letters* **1998**, *72*, 1173-1173.

45. Macdonald, J.R. Impedance spectroscopy, John Wiley, New York (**1987**).
46. http://www.tesatape.com
47. http://www.solartronanalytical.com/downloads/downloads.html
48. Falk, E.; Lacquet, B. M.; Swart, P. L. Determination of equivalent circuit parameters of porous dielectric humidity sensors. *Electronic Letters* **1992**, *28*, 166-167.
49. Jonscher, A.K. Analysis of the alternating current properties of ionic conductors. *Journal of Materials Science* **1978**, *13*, 553-562.
50. Jonscher, K. The interpretation of non-ideal dielectric admittance and impedance diagrams, *Physica Status Solidi (a)* **1975**, *32*, 665-676.
51. Fleming, W. J. A physical understanding of solid state humidity sensors. *Society of Automotive Engineers Transactions, Section 2* **1981**, *90*, 1656-1667.
52. Khanna, V. K.; Nahar, R. K. Surface conduction mechanisms and the electrical properties of Al_2O_3 humidity sensor. *Applied Surface Science* **1987**, *28*, 247-264.
53. Khanna, V. K.; Nahar, R. K. Carrier-transfer mechanisms and Al_2O_3 sensors for low and high humidities. *Journal of Physics D: Applied physics* **1986**, *19*, L141-L145.
54. Nahar, R.K.; Khanna, V.K.; Khokle, W.S. On the origin of the humidity-sensitive electrical properties of porous aluminum oxide. *Journal of Physics D: Applied Physics* **1984**, *17*, 2087-2095.
55. Nahar, R. K.; Khanna, V. K. Ionic doping and inversion of the characteristic of thin film porous Al_2O_3 humidity sensor. *Sensors and Actuators B* **1998**, *46*, 35-41.
56. Wood, G. C.; Skeldon, P.; Thompson, G. E.; Shimizu, K. A model for the incorporation of electrolyte species into anodic alumina. *Journal of the Electrochemical Society* **1996**, *143*, 74-83.
57. Patermarakis, G.; Moussoutzanis, K. Mathematical models for the anodisation conditions and structural features of porous anodic Al_2O_3 films on aluminum. *Journal of the Electrochemical Society* **1995**, *142*, 737-743.

Sample Availability: Available from the authors.